Theor Appl Climatol (2015) 122:315–335
DOI 10.1007/s00704-014-1300-2

ORIGINAL PAPER

Sensitivity of simulated extreme precipitation and temperature to convective parameterization using RegCM3 in China

Pinhong Hui · Jianping Tang · Shuyu Wang · Jian Wu

Received: 2 March 2014 / Accepted: 7 October 2014 / Published online: 17 October 2014

Abstract In this study, the regional climate model of RegCM3 is applied to investigate the sensitivity of regional climate over China using four cumulus parameterizations, the modified Anthes-Kuo (AK), the Grell with Arakawa-Schubert closure, the Grell with Fritsch–Chappell closure, and the MIT-Emanuel (EM). The model was integrated over the period of 1982 to 2001 using the NCEP Reanalysis data NNRP2 as boundary conditions. RegCM3 coupled with various cumulus parameterizations is evaluated firstly as for its ability to represent regional climatology and climate extreme indices, and the results show that simulated regional climate in China is sensitive to the option of cumulus parameterizations. All the cumulus schemes produce a northward expansion of heavy rain area and an underestimation of surface air temperature. For precipitation, the AK scheme simulates relatively better magnitude, while the EM scheme has more reliable performance on the spatial distribution. RegCM3 can represent the spatial distributions of extreme indices for both precipitation and temperature, as well as their decadal trends irrelevant to the cumulus parameterizations. However, the model underestimates the consecutive dry days and overestimates the three extreme wet indices, with the EM scheme giving the worst result. Slight underestimations of extreme temperature indices are detected in all cumulus parameterization scheme runs. The shapes of probability distribution functions for extreme indices are correctly produced, though the probabilities of extreme dry and warm events are underestimated.

P. Hui · J. Tang (✉) · S. Wang
School of Atmospheric Sciences, Nanjing University, 22 Hankou Road, Nanjing 210093, China
e-mail: jptang@nju.edu.cn

P. Hui · J. Tang · S. Wang
Institute for Climate and Global Change Research, Nanjing University, Nanjing 210093, China

J. Wu
Department of Atmospheric Science, Yunnan University, Kunming 650091, China

1 Introduction

Compared with global climate models, the regional climate models (RCMs) can better describe the mesoscale processes as well as the inhomogeneous landscape and complex topography, and therefore have been increasingly applied in the climate research on a regional scale (Fu et al. 1998; Lee and Suh 2000; Liu et al. 1994, 1996; Zhang et al. 2007). In previous studies, RCMs have been proven as valuable tools to provide reliable regional-scale information, especially in the areas where the climate is strongly regulated by underlying topography and the surface heterogeneity (Bonnardot and Cautenet 2009; Heikkila et al. 2011; Zhang et al. 2009). Many efforts have been made to apply RCMs to simulate the present climate and predict the future conditions over Asia (Dimri et al. 2013; Fu et al. 2005; Gao et al. 2002; Gu et al. 2012; Ho et al. 2011; Lee et al. 2013, 2014; Lee and Suh 2000; Liu et al. 1994; Sato and Xue 2013; Zhang et al. 2007). Some of these researches indicate that RCMs can simulate the spatial distributions and the linear trends of precipitation extremes well. RCMs' projections also show that the precipitation will become more "extreme" for the twenty-first century.

In regional climate models, precipitation is generated by both the grid-resolvable and sub-grid processes. The representation of sub-grid scale precipitation processes is known as the cumulus parameterization schemes (CPSs). Among all the physical parameterizations, CPS is considered as one of the most crucial to determine the RCMs' reliability. In the regional climate modeling, application

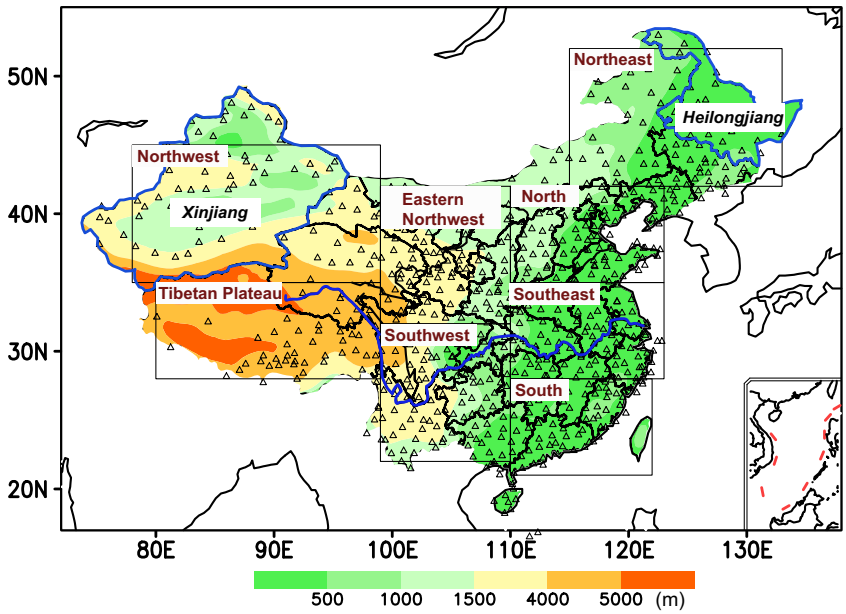

Fig. 1 Simulation domain and eight sub-regions (*circled by rectangles*). The regional topography is demonstrated in *color shadings* (unit: meters), and the surface observation stations are indicated with *triangles*. Three areas of Xinjiang, Heilongjiang, and the Yangtze River, which are mentioned in the paper, are highlighted by *blue lines*

of different CPS can lead to diverse simulation results. However, no single CPS is better than the others in simulation of regional climate, and a certain CPS's performance is region-dependent (Davis et al. 2009; Gianotti et al. 2011; Im et al. 2008; Kang and Hong 2008; Liu and Wang 2011; Mukhopadhyay et al. 2010; Ratna et al. 2014; Singh et al. 2006; Sinha et al. 2012; Tchotchou and Kamga 2009; Zanis et al. 2009). For example, the MIT-Emanuel scheme simulates more reliable rainfall intensity for the Indian summer monsoon, while the Grell scheme can produce better upper-air atmospheric circulation (Sinha et al. 2012). For the

Table 1 Experimental design and features of each experiment

Experiment identifier	Length of simulation	Specific points
AK	20 years (1982–2001)	1. Vertically integrated moisture convergence closure 2. Well designed for tropics and coarse-grid applications 3. Without convective downdrafts 4. Not suitable for mesh size applications
GAS	20 years (1982–2001)	1. Relates the convective fluxes and rainfall to the tendencies in the state of the atmosphere 2. Arakawa and Schubert closure 3. Constant mass flux with height 4. Downdraft processes 5. Ignores entrainment–detrainment effects 6. A statistical equilibrium between convection and the large-scale processes
GFC	20 years (1982–2001)	1. Relates the convective fluxes to the degree of instability in the atmosphere 2. Fritsch and Chappell closure 3. constant mass flux with height 4. downdraft processes 5. ignores entrainment-detrainment effects 6. a statistical equilibrium between convection and the large-scale processes
EM	20 years (1982–2001)	1. Auto-conversion of cloud water into precipitation inside cumulus clouds 2. The precipitation is added to a single, hydrostatic, unsaturated downdraft that transports heat and water 3. Transport of passive tracers

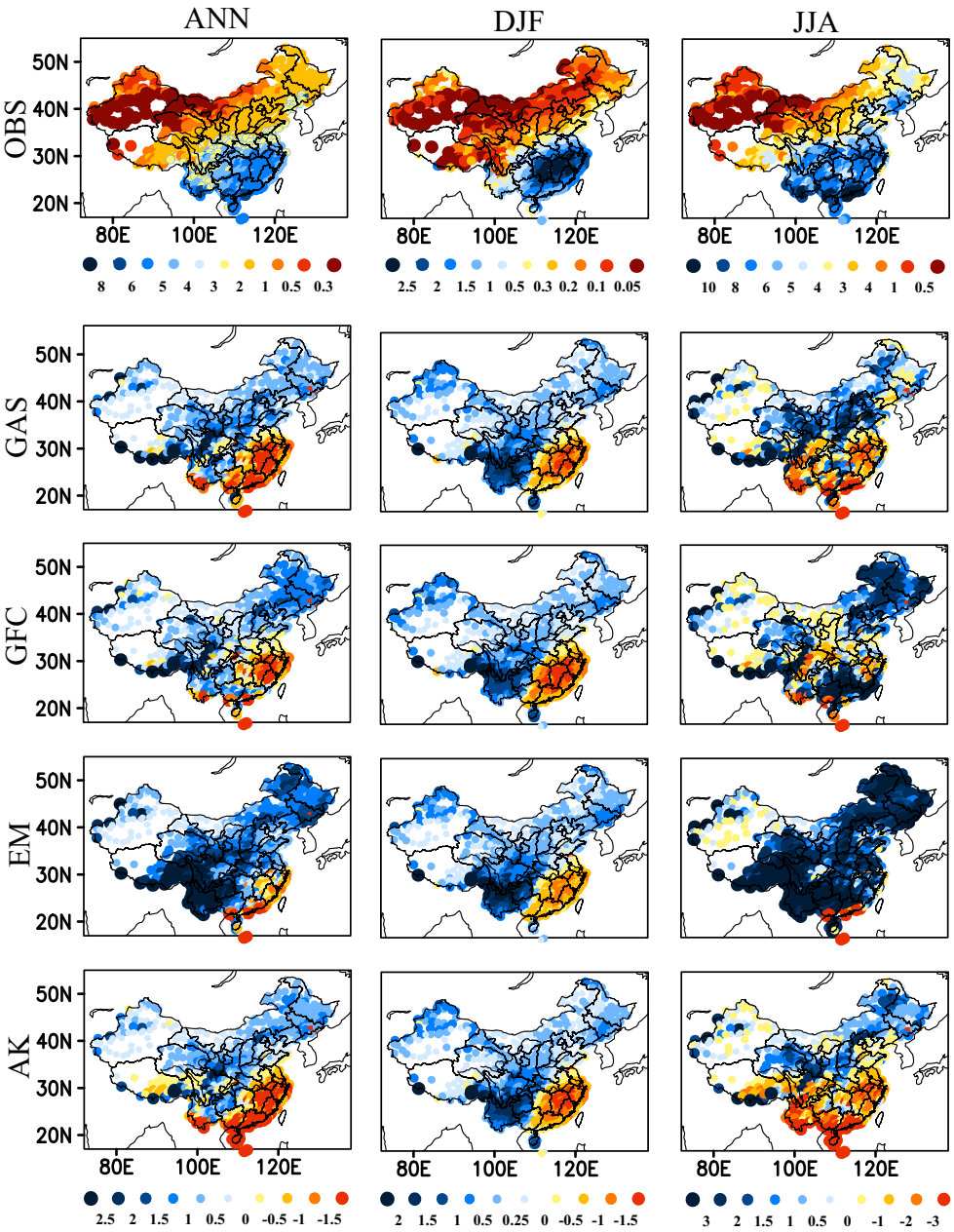

Fig. 2 The *top panel* demonstrates the 20-year (1982–2001) averaged spatial distributions of annual, DJF and JJA mean precipitation from APHRODITE (millimeters per day). From *second* to *bottom panel*, the biases of annual, DJF and JJA precipitation by four cumulus schemes of GAS, GFC, EM, and AK are illustrated

regional climate over Maritime Continent, the Grell scheme with Fritsch–Chappell closure can provide the best estimation for both the rainfall histogram and average diurnal cycle (Gianotti et al. 2011).

Compared with the climatology, the climate extremes are more sensitive to global change and have direct impacts on both natural environment and socio-economy. The changes in climate extremes as for their average and trend are regarded as one of the most crucial issues in global change research and receive much attention in both social development and climate-change communities (Alexander et al. 2007; Tank and Konnen 2003; Williams et al. 2010). As a result, the changes in both precipitation and temperature extremes are observed globally (Alexander et al. 2006; Choi et al. 2009; Goswami et al. 2010; Haylock and Nicholls 2000; Hegerl et al. 2004; Manton et al. 2001; Moberg and Jones 2005; Moberg et al. 2006; Tank et al. 2006; Yan et al. 2002). For monsoon China, the climate extreme events and their variances are analyzed systematically (Dong et al. 2011; Du et al. 2013; Fan et al. 2012; Gong et al. 2004; Hu et al. 2012; Li and Wang 2012; Qian et al. 2012; Su et al. 2006; Tian et al. 2012; Wang et al. 2012; Xu et al. 2011; Zhai et al. 2005; Zhang et al. 2011). In East China, the significant inter-decadal change of the precipitation extremes was detected over past 50 years

(1960–2009), and more precipitation extremes occurred during past 20 years (1990–2009) (Li and Wang 2012). The decreasing trend of light rain and increasing trend of extreme strong rain were detected for China during 1960–2000 (Qian et al. 2007). For the northwest China, temperature extremes showed a warming tendency and most precipitation indices exhibited increasing trend (Wang et al. 2013). Such changes in climate extremes have significant impacts on both ecosystem management and socio-economic development.

In this study, the numerical integrations are carried out for the time period of 1982–2001, and the impacts of cumulus schemes on regional climate as well as its inter-annual variability in different sub-regions of China are analyzed and presented. This study is featured with the regional variation of climatic response to CPSs, which received relatively little attention before. The performances of CPSs in RegCM3 in reproducing the regional climatology are evaluated first and then the model's sensitivity as for simulated climate extremes to various CPSs in China is investigated as well.

The paper is arranged as the following. In Section 2, the descriptions of RegCM3 model and the experimental design are provided. In Section 3, the analysis and evaluation of simulated mean climate and extremes by four CPSs are presented. Concluding remarks and discussion are given in Section 4.

2 Model description and experiment design

2.1 Model description

The regional climate model used in this study is the version 3 of Regional Climate Model RegCM3, which is developed and maintained by the International Centre for Theoretical Physics (Pal et al. 2007a). RegCM3 is used worldwide to simulate the regional-scale climatology and extremes, and provides insights into the regional climate processes. As compared with the previous versions (Giorgi et al. 1993a, b), RegCM3 includes a number of new features including improvements to the physics packages that enhance model performance in

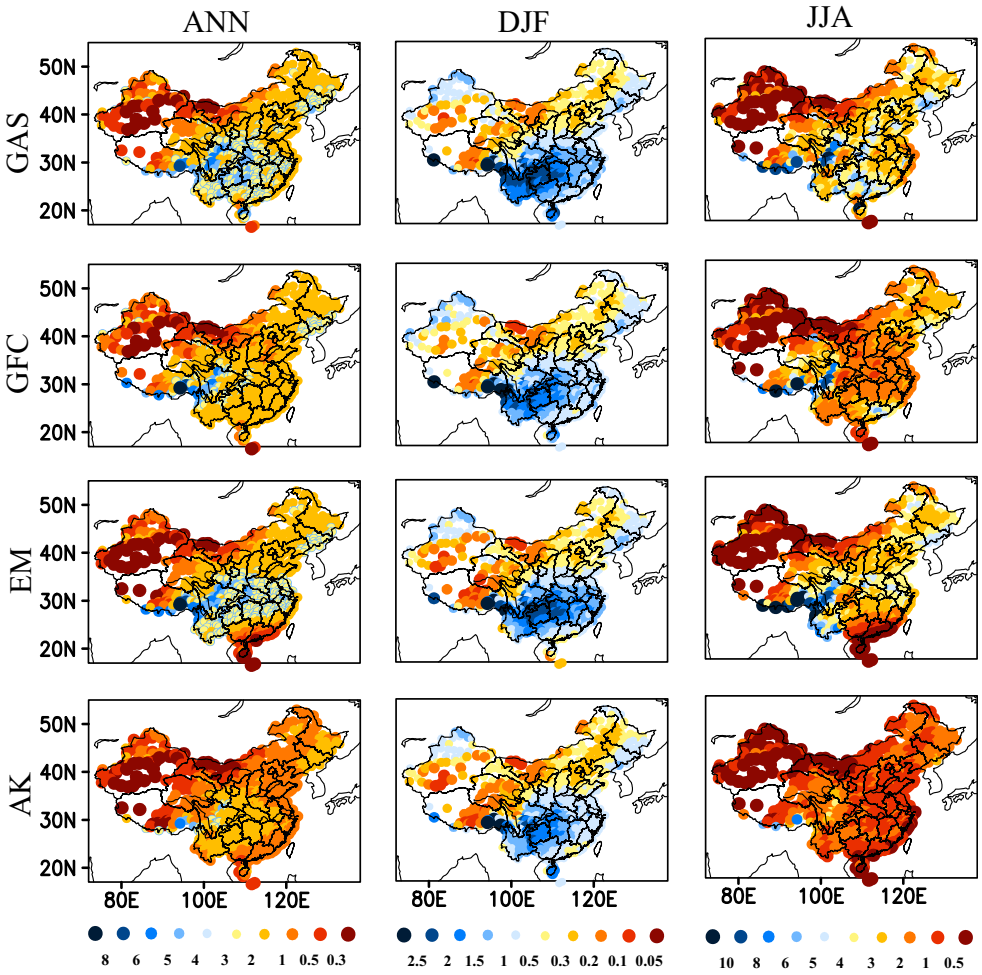

Fig. 3 Spatial distributions of 20-year (1982–2001) averaged annual, DJF and JJA large-scale precipitation (millimeters per day). From *top* to *bottom panel*, the simulation results with four cumulus schemes of GAS, GFC, EM, and AK are illustrated

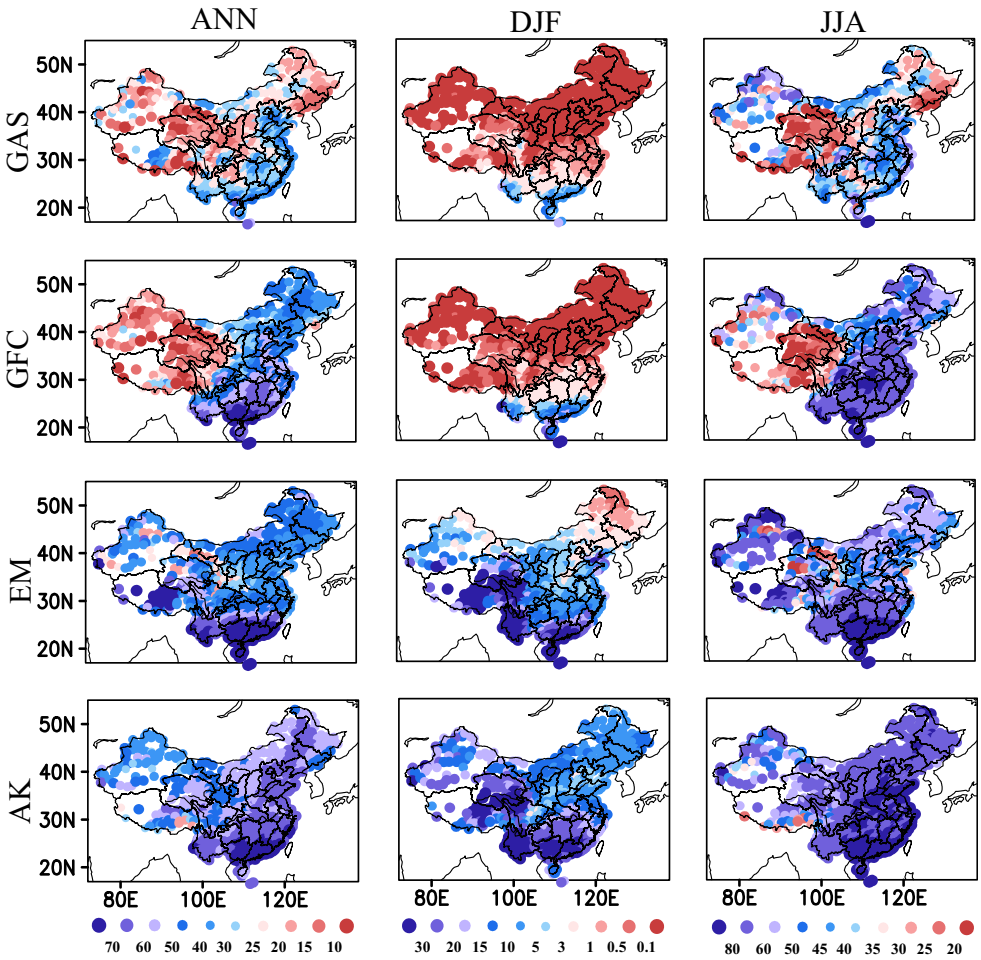

Fig. 4 The same as in Fig. 3, but for the convective rain fractions (%). The fraction is represented by the ratio of the convective to total rainfall amount in percentage

tropical and subtropical regions. The model can be interfaced with a wide range of large-scale boundary driving fields (Pal et al. 2007b). RegCM3 contains four options of cumulus and closure parameterization schemes, namely the modified Anthes-Kuo (Anthes 1977), the Grell scheme (Grell 1993) implemented with the Arakawa and Schubert closure (Grell et al. 1994), the Fritsch and Chappell closure (Fritsch and Chappell 1980), and the MIT-Emanuel scheme (Emanuel 1991; Emanuel and Zivkovic-Rothman 1999), which is newly integrated within RegCM3.

2.2 Experiment setup

In this study, RegCM3 was run centered at (35°N, 105°E) (Fig. 1). The domain has a mesh size of 91×110 with a horizontal resolution of 50 km. In the vertical direction, 18 levels were defined unequally from surface to the model top at 50 hPa. Major physics parameterization schemes used in this study include the CCM3 radiation scheme (Kiehl et al. 1996), the BATS land surface model (Dickson et al. 1993), and the PBL scheme developed by (Holtslag et al. 1990). According to various climate characteristics, eight sub-regions (i.e., northeast, north, eastern northwest, northwest, southeast, south, southwest, and Tibetan Plateau) are adopted for analyzing the effects of CPSs on regional climatology and extremes.

Four groups of 20-year integration applying different choices of the cumulus schemes are carried out and referred to as the modified Anthes-Kuo (AK), Grell with Arakawa-Schubert closure (GAS), the Grell with Fritsch-Chappell closure (GFC), and the MIT-Emanuel (EM) in the paper (Table 1). The features of each experiment are described in Table 1 as well. For large-scale cloud and precipitation scheme, SUBEX scheme (Pal et al. 2000) is applied for all four experiments.

2.3 Data for validation

The simulation results obtained from four integrations are evaluated against the station observations of daily precipitation, daily mean, and maximum and minimum surface air

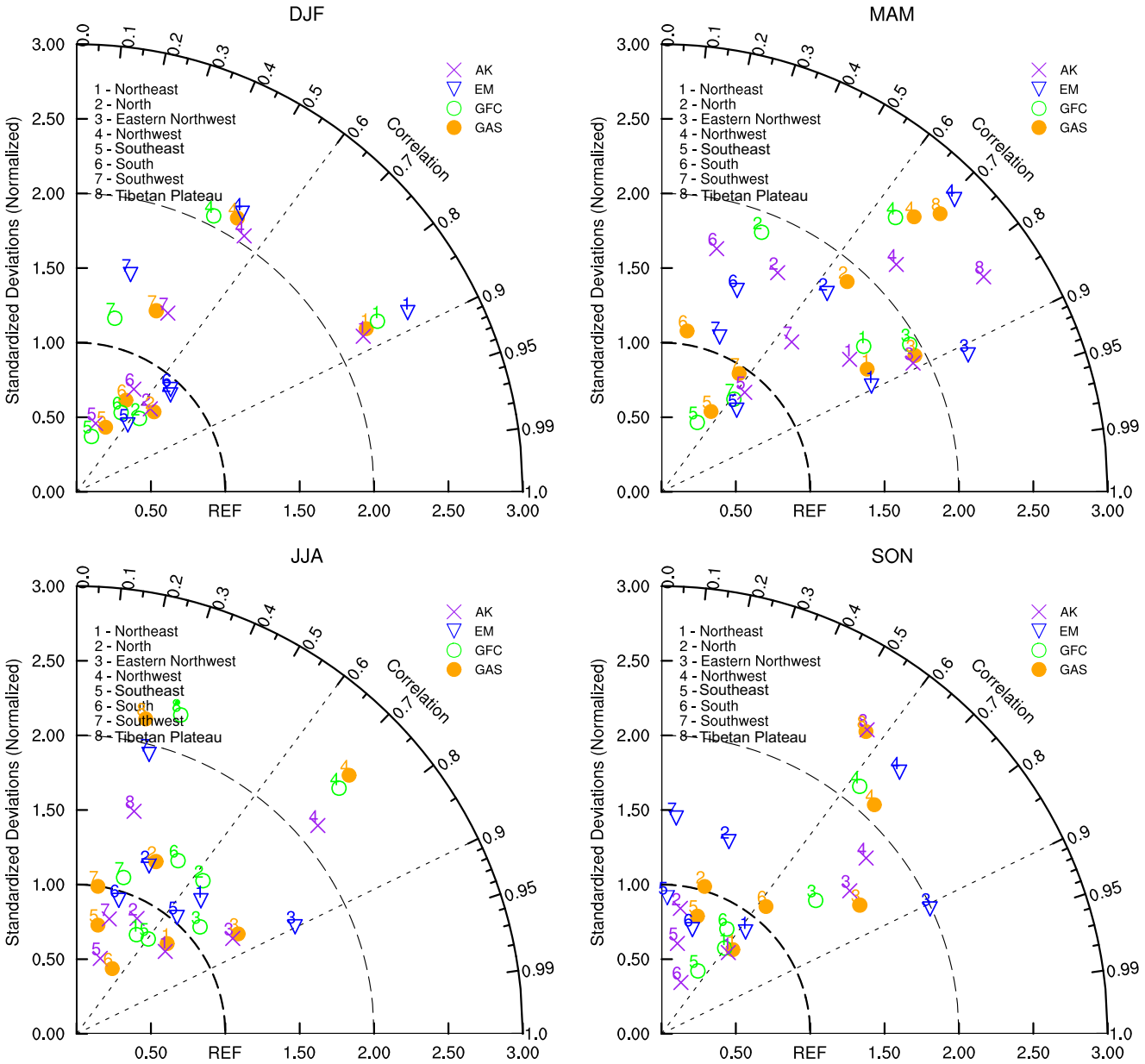

Fig. 5 Taylor diagram of statistical analysis for different CPSs in simulating seasonal mean precipitation in different sub-regions of China. The cumulus schemes of AK, EM, GFC, and GAS are represented by different symbols. For each point, the radial distance from the origin to the point is the ratio between simulated and observed standard deviation of the spatial pattern for seasonal precipitation averaged during 1982–2001. The azimuthal position gives the spatial correlation coefficient between the two fields

temperatures. The surface observations are provided by the China Meteorological Administration, which are obtained from the observational network consisting of 756 meteorological stations covering the whole country.

3 Results

The RegCM3 results with four options of CPSs are firstly interpolated onto the station locations with bilinear interpolation method and then evaluated against the daily observation to assess the capacity of different CPSs to reproduce the China's surface climatology as well as extremes.

Fig. 6 Simulated and observed probability distribution function (PDFs) ▶ of daily precipitation calculated for different sub-regions over China, **a** winter and **b** summer. The results of observation and simulations from four CPS runs are represented by color bars (*orange*, GAS; *green*, GFC; *blue*, EM; *purple*, AK; and *black*, observation)

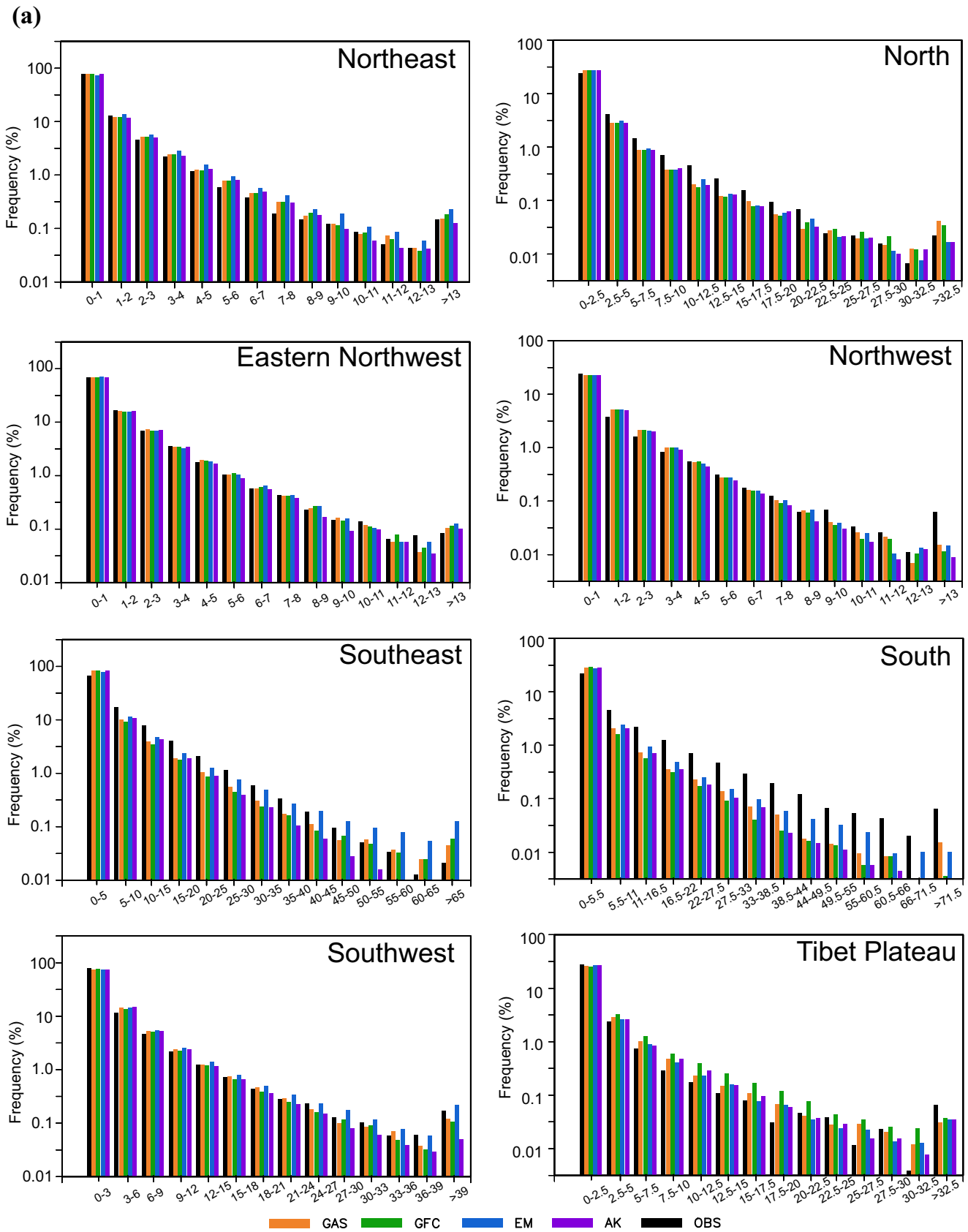
(a)
Northeast
North
Eastern Northwest
Northwest
Southeast
South
Southwest
Tibet Plateau
Frequency (%)
GAS
GFC
EM
AK
OBS

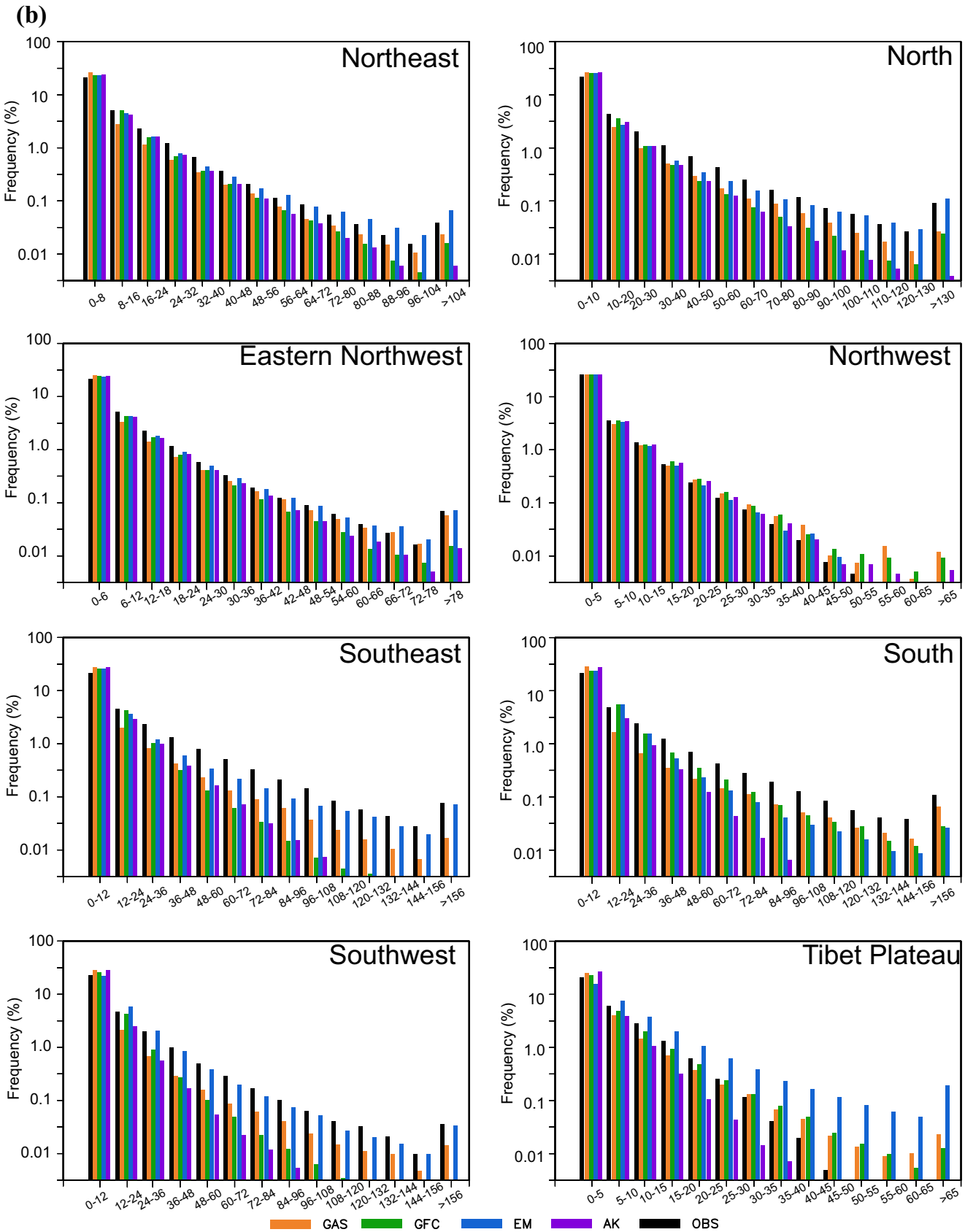

Fig. 6 (continued)

3.1 Surface climatology

3.1.1 Precipitation

As shown in Fig. 2, both the observed annual and seasonal mean precipitations demonstrate the geographic gradient of increasing wetting southeastwards, and all four CPSs can reproduce these main characteristics (figures not given). Comparing the simulated annual mean precipitation with the observation, it can be seen that all CPSs present overestimation over the arid and semi-arid parts of China, when they produce less rainfall along the southeast coast. Among all the schemes, AK shows the smallest overestimation while the EM scheme performs the worst especially over the northeast and southwest China. In winter, all the CPSs display a significant overestimation of precipitation over southwest China and underestimation over southeast China. The simulated summer rainfall intensities and spatial patterns from four CPSs runs are different from each other. The EM scheme overestimates the rainfall intensity most greatly over almost the whole country, and AK displays underestimation over the southeast China.

The large-scale precipitation and ratio of convective to total precipitation amounts is shown in Figs. 3 and 4, respectively, with the purpose of understanding the effect of CPSs on the regional precipitation. Although applying the same grid-resolvable scheme, the large-scale precipitations produced in four CPS runs demonstrate the discrepancy with respect to both rainfall intensity and spatial distribution (Fig. 3). This is because CPS affects the latent and sensible energy balance, changes the thermal and dynamic condition in the atmosphere, and therefore modulates the large-scale circulation and the large-scale precipitation. The convective precipitation ratios from four CPSs runs decrease from southeast to northwest part of China (Fig. 4). Comparably, AK gives the largest percentage of subgrid-scale rainfall while it produces the smallest non-convective precipitation. GAS and GFC, on the other hand, produce a smaller percentage of convective precipitation than the other two schemes. Similar conclusions have been drawn in the previous studies with disregard to the single MCS rainstorm simulations (Kuo et al. 1996; Wang and Seaman 1997; Yang et al. 2000) and regional climate simulations (Lee et al. 2005). For the annual precipitation simulated by the EM scheme, the convective precipitation dominates over the south part of China while it balances with the large-scale precipitation in other regions. Regarding the seasonal mean results, strong convection and accompanying large convective precipitation in summer are well captured by all CPSs. AK's less non-convective precipitation and larger percentage of subgrid-scale rainfall reveals that its underestimation of total precipitation is due to the dry bias of large-scale precipitation. In winter, the convective effect is relatively weak, especially for the GAS and GFC simulations.

Using Taylor's diagram, the statistic, including the spatial correlation and spatial variability, of seasonal mean precipitation by four CPSs in different sub-regions of China is provided (Fig. 5). In Taylor's diagram, the spatial variability is represented by the ratio of the simulated and observed standard deviations of the spatial distributions for seasonal precipitation. Over the northern sub-regions, the spatial correlation coefficients ($\geq$0.28) between simulated and observed precipitation are statistically significant at 95 % confidence level for all CPSs, revealing that all four CPSs are capable of simulating the spatial distributions of precipitation over higher latitude which is demonstrated in Fig. 3. Over most sub-regions, EM has better performance than the other schemes in spring, summer, and autumn. But in winter, AK shows some superiority in generating the spatial patterns.

To gain more insight into the difference among CPSs' performances, the observed and simulated probability distribution functions (PDFs) of daily precipitation for both summer and winter seasons are calculated (Fig. 6). For summer precipitation, in the sub-regions of northeast, eastern northwest, and northwest China, CPSs can reasonably reproduce the probability distribution with little inter-scheme diversity. Meanwhile, relatively large inter-scheme discrepancy is simulated in the other sub-regions. In north, southeast, south, and southwest China, all schemes overestimate the light rain and underestimate the high-intensity precipitation. The skill of GFC is relatively better for south China, as EM for the other three sub-regions with its PDF spectrums are closest to the observation. AK performs poorly with the largest underestimation for high-intensity rainfall, missing the extreme precipitation larger than 120 mm/day all together. In the Tibetan Plateau, GAS and GFC perform better than the other two schemes. However, AK produces more light rain and less heavy rain than the observation, and EM gives the adverse results. The probability distributions of winter precipitation for northeast, north, eastern northwest, northwest, and southwest China are all well produced. The spectrums of winter precipitation for southeast and south China are similar to those of summer. In Tibetan Plateau, the higher end of rainfall spectrum is overestimated by all CPSs.

3.1.2 Surface air temperature

Similar to the simulated precipitation from four CPSs, the surface air temperature also show discrepancy due to the model's integration with CPS (Fig. 7). All schemes represent reasonably the spatial patterns of seasonal mean surface air temperature, underestimation and little discrepancy is found among the four CPSs. The cold bias of RegCM3 is likely to be systematic, which has been detected in many researches (Davis et al. 2009; Im et al. 2008; Pal et al. 2007b) and may be caused by the model's excessive precipitation.

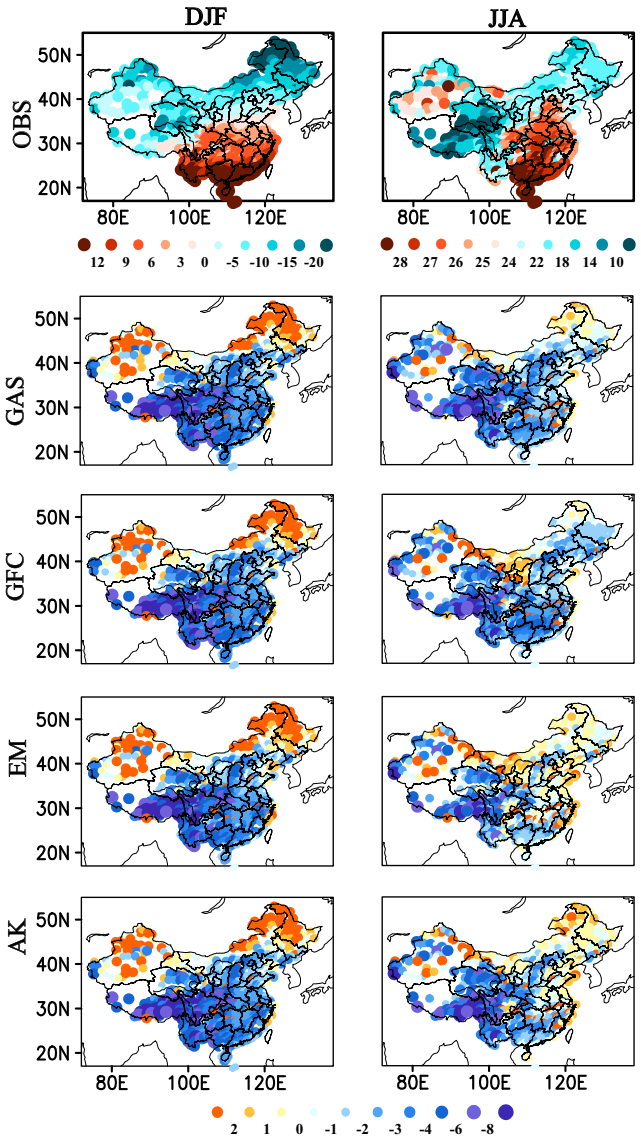

Fig. 7 The same as in Fig. 2, but for the spatial distributions of seasonal surface air temperature averaged over 1982–2001 (degrees Celsius)

The spatial correlation and standard deviation analyses (Fig. 8) show that, for cooler seasons, namely winter, spring, and autumn, CPSs can produce more reliable surface air temperature which have statistically significant correlation coefficients (at 95 % confidence level) with the observation. It indicates that CPSs have little effect on model's performance of the cooler season's averaged surface temperature as the weaker convection during cooler seasons triggers little change in the vertical heating profile. As for the sub-regional variation, the seasonal temperature induced by CPSs has smallest correlation with the observation over southeast and south China, especially for the summer season when convective activities are stronger. The results suggest that the convection-induced sub-grid circulation can affect the regional heating budget, and the accurate description of convective activities is necessary to reproduce the temperature.

The standard deviation of seasonal averaged temperature is underestimated for most CPSs experiments over most sub-regions, except for northwest and southwest China. Generally, CPSs' effect on the spatial variability of seasonal temperature may depend on the climate-regime, as CPSs tend to have better agreement with each other over drier region. Comparably, CPSs' simulations of the spatial variability of seasonal temperature are relatively more reliable over regions with the homogenous land surface, such as north and northwest China. The largest underestimation of the spatial variability of seasonal temperature appears over the Tibetan Plateau, and in the southeast, south, and northeast China, indicating that the interactions and feedbacks between complex terrain and regional convective process may induce great impact on the climate variabilities.

In order to further understand performance of the four cumulus schemes in simulating surface air temperature, the simulated and observed PDFs for all sub-regions are shown in Fig. 9. For winter season, the bell-shaped patterns in most sub-regions are well captured, though all CPSs induce the shift towards low temperature over the low-latitude sub-regions (southeast region, south and southwest China, and the Tibetan Plateau). For summer season, relatively large discrepancy among four schemes appears over low-latitude sub-regions, and similar to that of winter season, a shift towards lower temperature is simulated by all CPSs. Comparably, the EM scheme manifests significant advantage in reproducing the PDF of seasonal temperature. The shift of simulated PDFs of temperature to colder end is in accordance with the cold bias discussed in the beginning of this section, and it is more conspicuous over four low-latitude sub-regions. This is likely due to the excessive regional precipitation which may cause cloud feedbacks in east, south, and southwest China. Meanwhile, though the precipitation being overestimated in northern sub-regions, less regional total precipitation leads to weaker impact on probability distribution of temperature.

In summary, CPS is important to the temperature simulation over southeast and south China, and Tibet, especially for wetter and warmer seasons. Such result indicates that the further improvement should be made to better describe the complicated interactions and feedbacks between large-scale monsoon circulation and meso-scale circulation induced by convective activities and complex terrain. Comparably, the seasonal temperature over high-latitude regions is less sensitive to CPSs.

3.2 Extreme indices

To assess the model's ability to simulate the intensity, frequency, and duration of precipitation and temperature

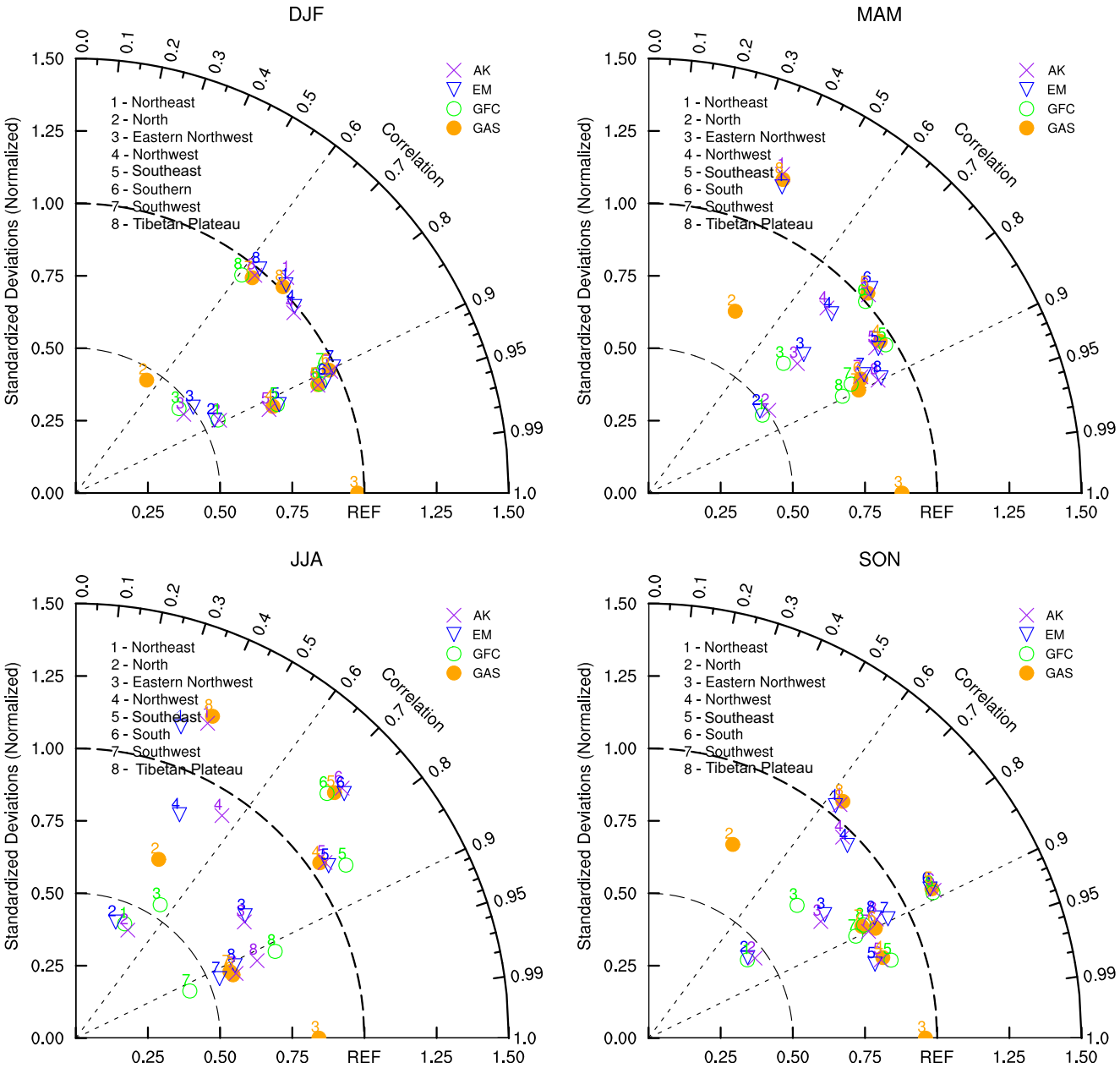

Fig. 8 The same as in Fig. 5, but for surface air temperature

events on regional scale, totally eight extreme indices for both precipitation and surface air temperature are generated and presented. The decadal trend and probability distribution function for extreme indices are analyzed as well. Four indices are used to demonstrate the regional characteristics of precipitation extremes (Wang et al. 2013), that is, consecutive dry days (CDD), number of heavy precipitation days (R10), maximum 5-day precipitation amount (Rx5), and very wet days (R95). Their definitions are given in Table 2. For temperature extremes, the indices of summer day (SU), consecutive frost days (CFD), growing season length (GSL), and extreme temperature range (Moberg et al. 2006) are used, definitions of which are listed in Table 3.

3.2.1 Extreme rainfall

As shown in Fig. 10, CPSs produce the similar spatial distributions for all extreme indices. Comparing to the observation, all CPSs underestimate CDD by more than 20 days for dry and semidry China and by 0–20 days over Sichuan Basin, and overestimate CDD over southeast China by around 10 days.

For observed precipitation extreme indices of R10, Rx5, and R95, their spatial distributions follow that of annual mean

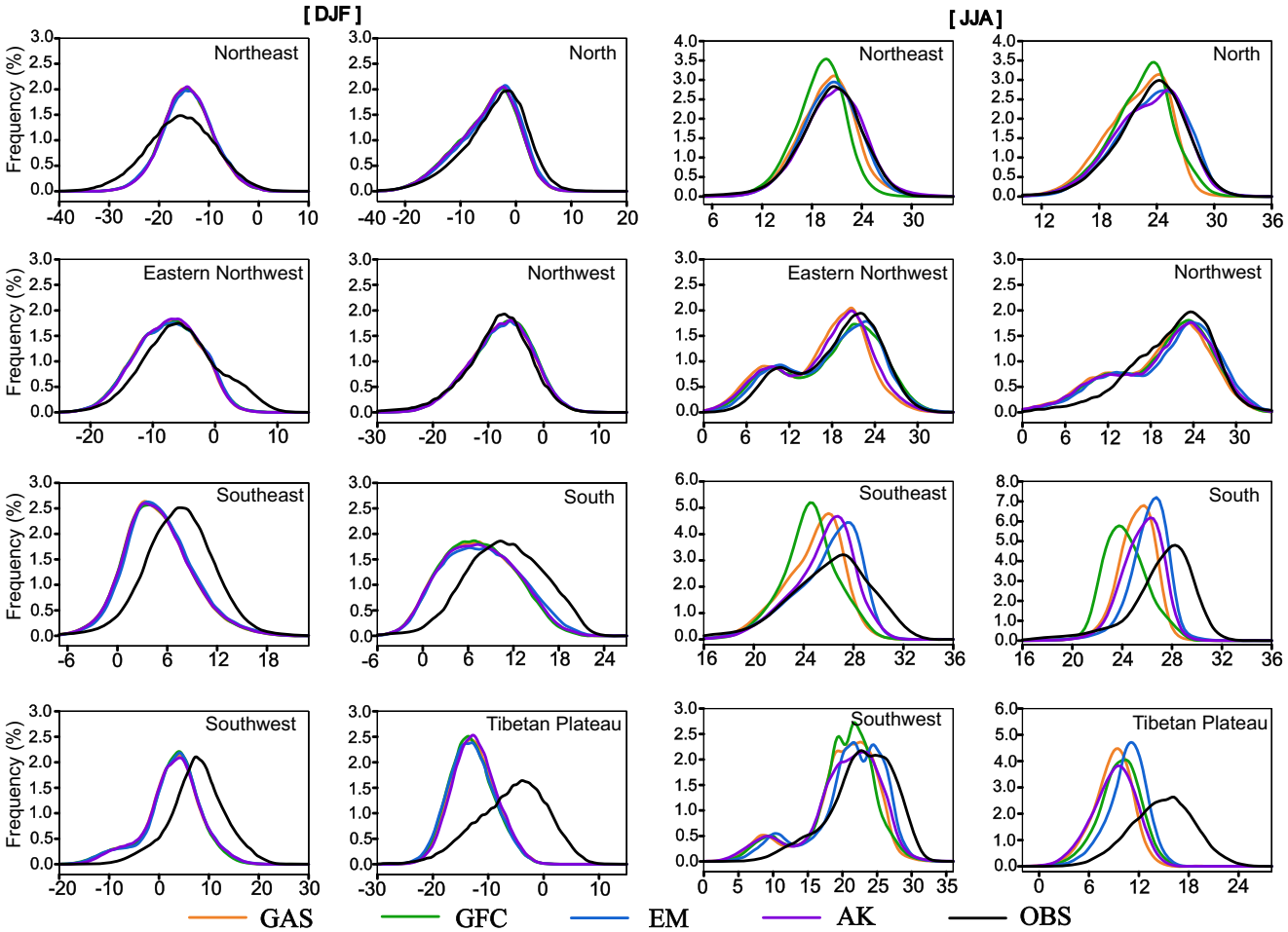

Fig. 9 Simulated and observed probability distribution function (PDFs) of daily surface air temperature for different sub-regions over China. The *first two columns* are results for winter and the *last two columns* for summer. The results of observation and simulation from four CPS runs are represented by color lines (*orange*, GAS; *green*, GFC; *blue*, EM; *purple*, AK; and *black*, observation)

precipitation and show clearly influence of monsoon system, as more precipitation extremes occur in southeast China and less in northwest China. All four CPSs can represent the spatial distributions of precipitation extreme indices, but they overestimate the heavy rainfall over arid and semi-arid regions of north, northwest, and northeast China. Over monsoon region of southwest, south, and southeast China, EM overestimates the precipitation extreme indices, which is in agreement with its overestimation of annual mean precipitation. GAS excessively overproduces R95 over almost the whole China, when it gives only moderate overestimation for mean precipitation over northwest part of China. Figure 6 shows that, over the sub-regions of northeast, east part of northwest, southeast, south, and southwest China, GAS produces higher frequencies of both drizzle to light rain and heavy rainfall than the other schemes, while its moderate rain has much lower frequency. The precipitation from GAS scheme therefore is more polarized, and as the result, excessive R95 is produced when the total precipitation is moderate.

The decadal trends of extreme precipitation indices show relatively large spatial inhomogeneity (Fig. 11). The observed CDD increases in most part of simulation domain above

Table 2 Definition of the extreme precipitation indices

Variable name	Definition
Consecutive dry days (CDD)	Maximum number of consecutive days with precipitation <1 mm
Number of heavy precipitation days (R10)	Annual number of days when Precipitation ≥10 mm
Maximum 5-day precipitation amount (Rx5)	Annual maximum consecutive 5-day precipitation
Very wet days (R95)	Annual total precipitation when precipitation >95th percentile

Table 3 Definition of the extreme temperature indices

Variable name	Definition
Summer day (SU)	Daily maximum temperature over 25 °C
Consecutive frost days (CFD)	Maximum consecutive days with daily minimum temperature below 0 °C
Growing season length (GSL)	The number of days between the first occurrence of at least six consecutive days with daily mean temperature above 5 °C and the first occurrence after 1st July of at least six consecutive days with daily mean temperature below 5 °C
Extreme temperature range (Moberg et al. 2006)	The difference between the annual maximum daily maximum temperature and minimum daily minimum temperature

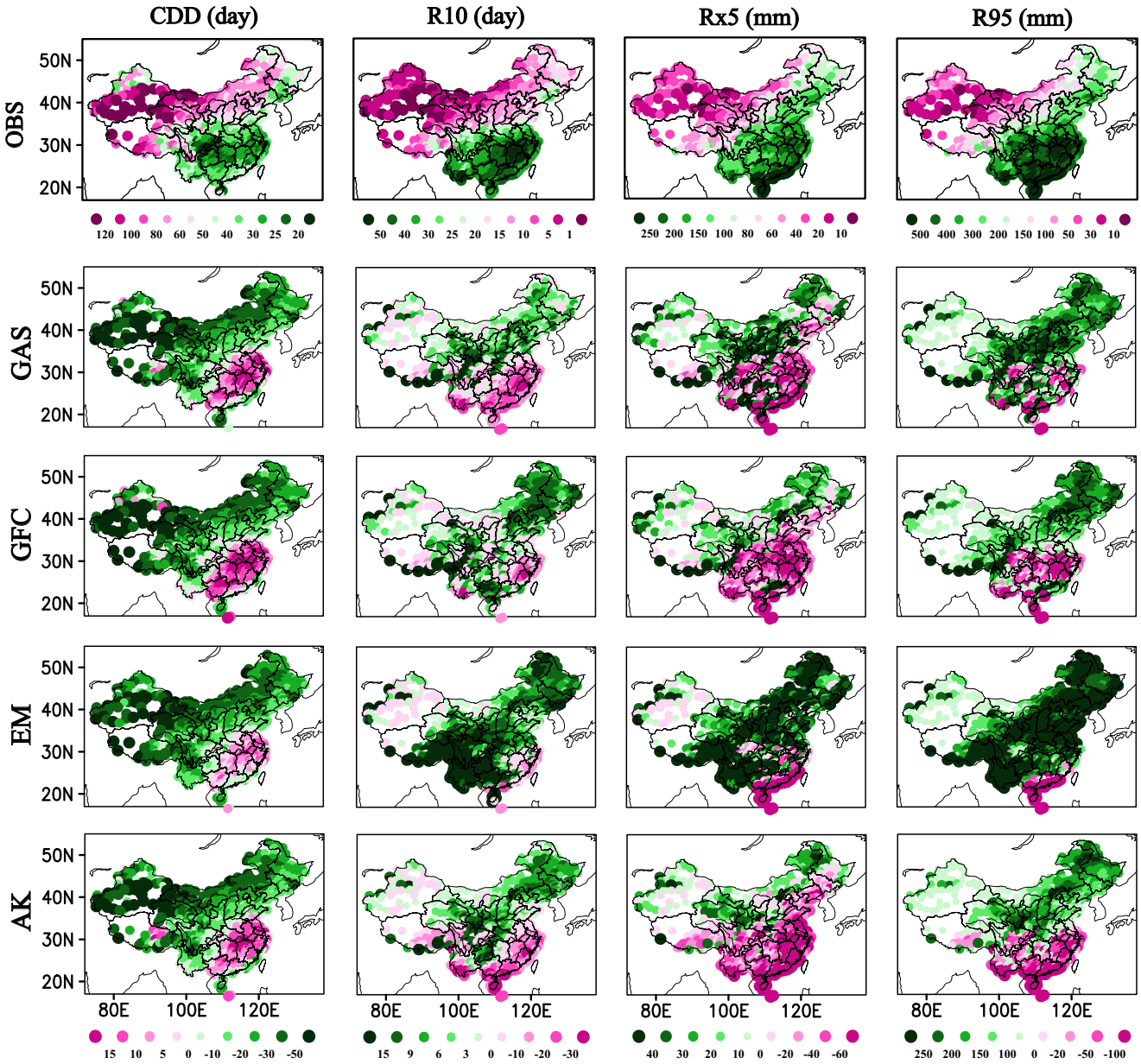

Fig. 10 The *top panel* is the observed spatial distributions of extreme precipitation indices averaged over 1982–2001 (millimeters per day). From *second* to *bottom panel*, the biases of extreme precipitation indices produced by four CPS runs of GAS, GFC, EM, and AK are illustrated. From *left* to *right column*, CDD, R10, Rx5, and R95 are shown, respectively

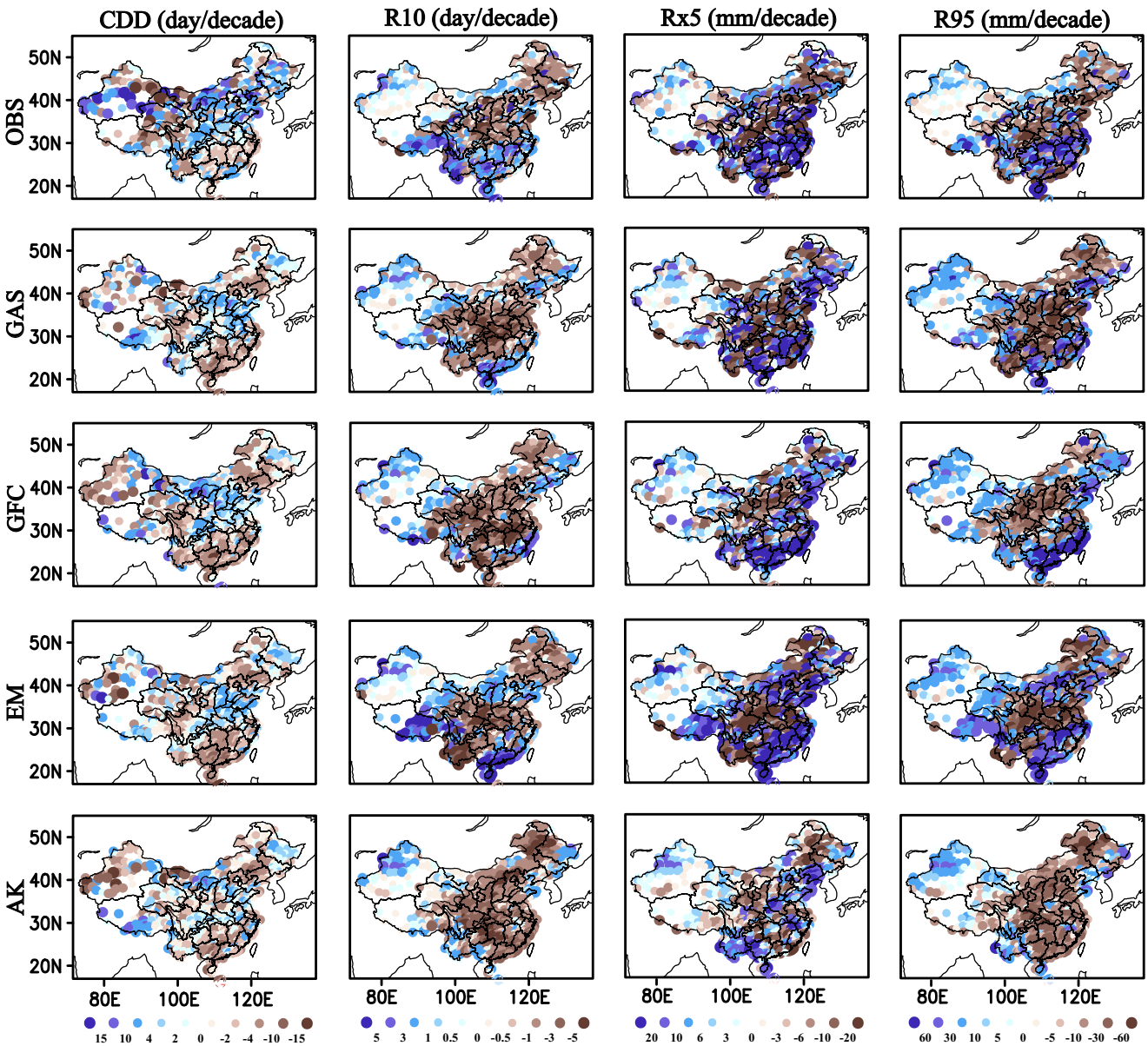

Fig. 11 The spatial distributions of decadal trends of extreme precipitation indices during 1982–2001. From *top* to *bottom panel*, the observation and results from four CPS runs of GAS, GFC, EM, and AK are illustrated. From *left* to *right column*, indices of CDD, R10, Rx5, and R95 are shown, respectively

35°N, indicating the intensifying dry tendency during 1982–2001 over most part of north China. Such drying tendency is verified by the trends of R10 and R95, which show clear reduction over most part of Center China, northeast China, and some part of north China. On the other hand, the observed light rain represented by Rx5 decreases along the transition zone between semi-arid region and Sichuan Basin. For the southern part of China, it can be concluded that the region has the wetting tendency during past decades (1982–2001), which is indicated by the decreased CDD and increased R10, Rx5, and R95 in the surface observation. In addition, the observed trends of extreme precipitation indices are significant at 95 % confidence level in most parts of China except over western Tibet and the very northeast China (figure not given).

Comparing the four extreme precipitation indices, the trends of CDD and Rx5 are better presented spatially than R10 and R95 in CPSs runs, and geographically, CPSs' abilities to simulate the extreme precipitation indices are more reliable over high-latitude region. Analyzing the simulated CDD, it can be seen that all CPSs reduce the duration of dry bell over northern part of China by underestimating the increasing trends or even giving the opposite tendency. For southern part of China, CPSs overestimate the decreasing trends of CDD, that is, CPSs weaken the wetting tendency of the observation. For

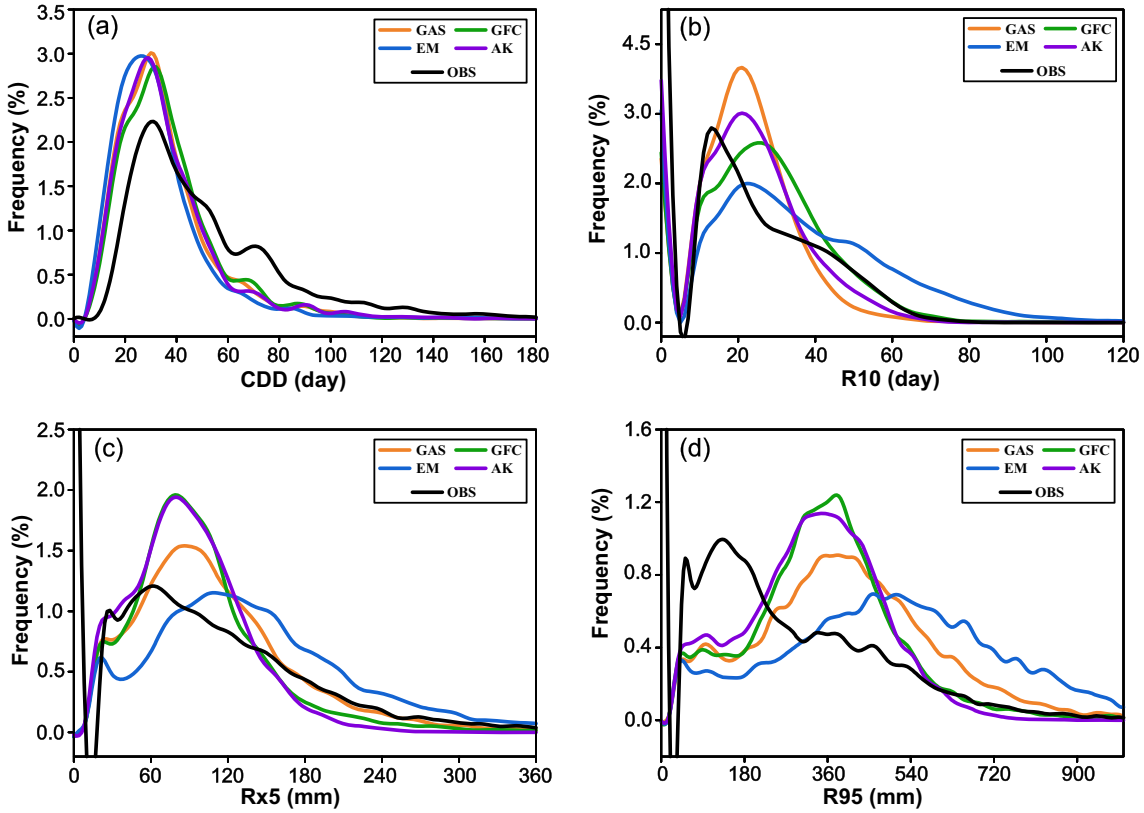

Fig. 12 Probability distribution functions for **a** CDD, **b** R10, **c** Rx5, and **d** R95. For CDD and R10, bin size of 1.0 day is used; and for Rx5 and R95, bin widths of 2.0 and 4.0 mm are used, respectively

R10 and R95, all CPSs overestimate the decreasing trends over northern part of China, and AK reduces the heavy rainfall and rainy days over southern part of China. In summary, CPSs runs can reproduce the drying tendency over northern part of China and wetting tendency over southern part of China, though, in all CPS simulations, the strength of both tendencies are weakened.

From PDF distributions of extreme precipitation indices (Fig. 12), it can be seen that the shape of PDFs is correctly produced, except for R95. However, the spectrums are shifted, and the magnitudes of peak values are misestimated. For the CPSs' CDD, the simulated histograms are shifted towards low values, suggesting that all CPSs underestimate the dry events. The histograms of the R10, Rx5, and R95 show the overestimation for extreme precipitation events by all CPSs. For Rx5 and R95, AK and GFC's results are close to each other, and EM overestimates the frequency of high value for both Rx5 and R95. GAS is differentiated from GFC only by the closure scheme, but it gives relatively worse performances as for PDF of Rx5 and R95.

3.2.2 Extreme temperature

From Fig. 13, it can be seen that the observed extreme temperature indices show similar spatial distributions as that of annual mean surface temperature. In general, four CPSs show abilities to reproduce the observed spatial patterns of extreme temperature indices. The CFD is overestimated, and GSL is underestimated by all CPSs, implying that RegCM3 has a systematic cold bias irrelative to model's treatment of convection. In all CPSs, EM gives a better production for GSL by producing smaller underestimation. For ETR, CPSs have slightly underestimation especially in Xinjiang and northeast China. Examining the biases of annual maximum and minimum temperature, it is found that both maximum and minimum temperatures are overestimated. But the larger warm bias in minimum temperature causes the discrepancy of ERT in all CPSs runs.

Due to the impact of global warming, the significant trends of longer summer days (SU), extended growing season (GSL), and shorter frost days (CFD) can be detected in the observation during past 20 years over most of simulation domain (Fig. 14). These trends of temperature extreme indices are significant at 95 % confidence level. The cumulus schemes generally produce similar spatial patterns of SU's trend to that of observation, except that they reduce the intensity of increasing trend over the region east of 105°E and generate a decreasing trend over northwest and southwest China. The overall decreasing trend of CFD is relatively well captured by all CPSs, though GAS, GFC, and EM have an

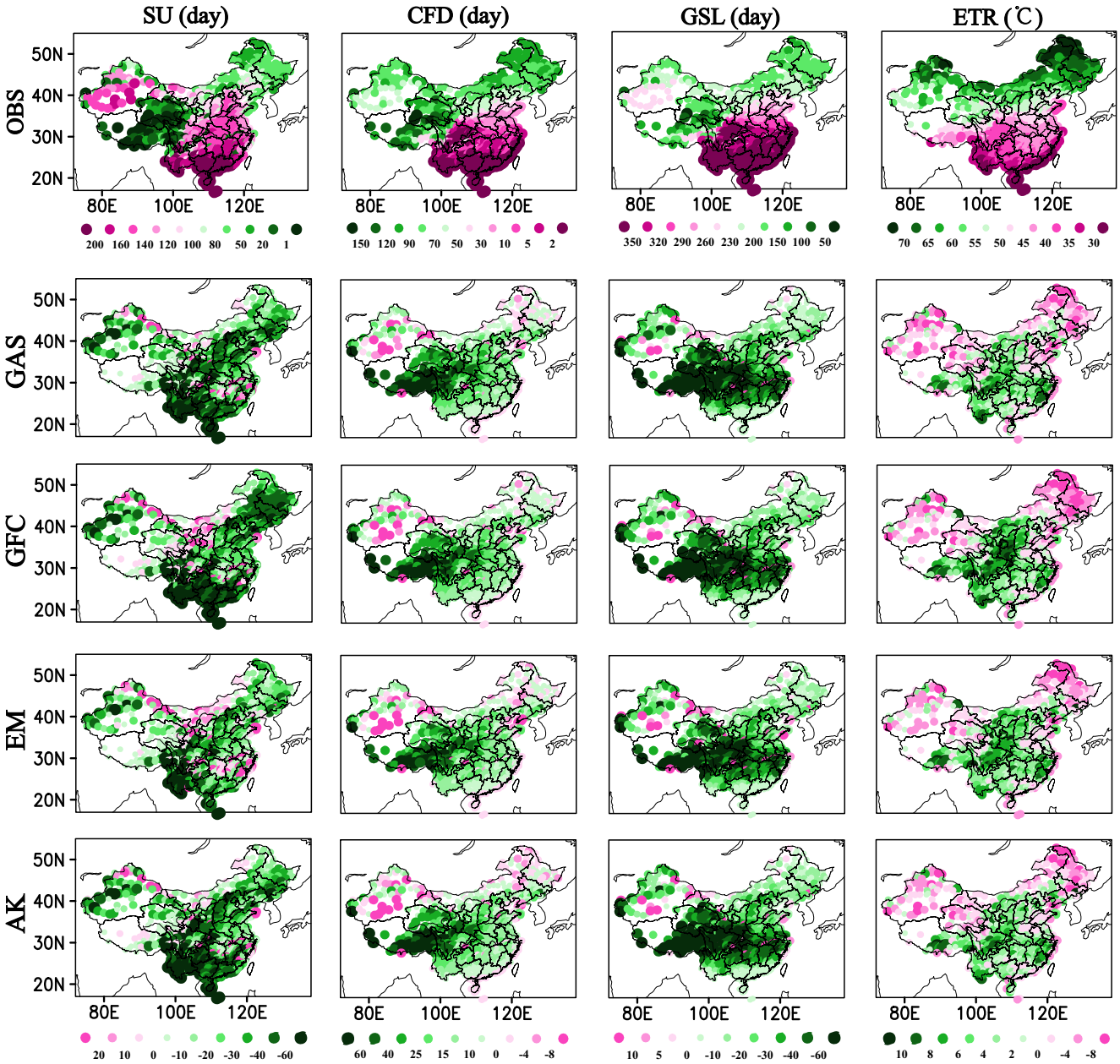

Fig. 13 The same as Fig. 10 but for the extreme temperature indices of SU, CFD, GSL, and ETR

opposite trend over the southwest China. The observed increasing trend of GSL is missed in all CPS runs over the most of simulation domain, except for the Yangtze River Basin, and northeast and south China.

From observation, the increasing trend of temperature range is the most significant over north China except over Heilongjiang, southern Xinjiang, and Tibet. All the four schemes show considerable skill in simulating the observed spatial pattern of ETR, though they overestimate the positive trends over high-latitude region. Both observed and simulated ETR demonstrate the opposite trends between over north China and over south part of Xinjiang and south China. The phenomenon is related to the different responses of average and extreme temperatures to the regional warming. As the average temperature increases during the simulation period, over the north part of the domain, the maximum temperature increases and minimum temperature decreases, leading to a larger ETR, while for the south part of the domain, the combined effect of decreasing maximum temperature and increasing minimum temperature results in the reduction of ETR.

Figure 15 shows the PDFs for extreme temperature indices. Regionally, the PDFs of extreme temperature indices are not

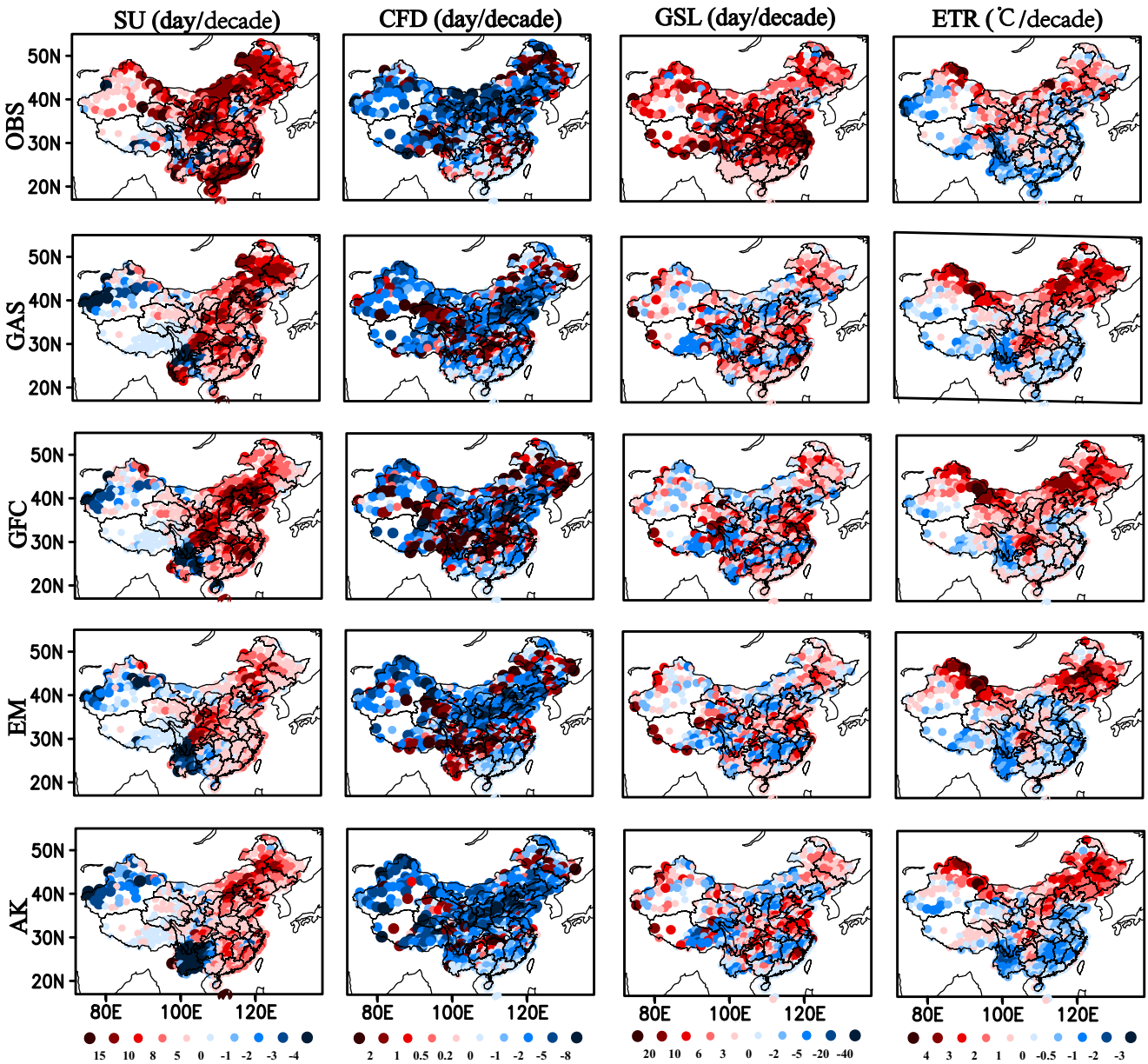

Fig. 14 The same as in Fig. 11, but for decadal trends of SU, CFD, GSL, and ETR

sensitive to CPSs. The shifting of SU and GSL's spectrums toward lower values in CPSs runs indicates underestimations for the extreme warm events. The higher ends of CFD and ETR spectrums are overestimated in all experiments, implying more extreme cold days and larger range of temperature. Comparably, AK and EM perform slightly better for CFD and ETR.

4 Conclusions and discussion

In this study, the sensitivity of the regional climate to the cumulus convection options over China is simulated using RegCM3. Four different cumulus and closure parameterization schemes, i.e., AK, GAS, GFC, and EM, are applied in four sets of 20-year (1982–2001) integration, respectively, while the rest of model's physical packages remain unchanged. The focus is laid on the extreme features of precipitation and surface air temperature before which an evaluation on mean climatology is also given. The priority of this study is to investigate the sensitivity of both regional climatology and extremes to the model's treatment of cumulus convection over China, which is influenced by monsoon climate variabilities at different scales and characteristic of complex landscape and terrain.

The results show that the simulations of the regional climate over China are sensitive to the choice of cumulus parameterization and closure schemes. Four CPS schemes are

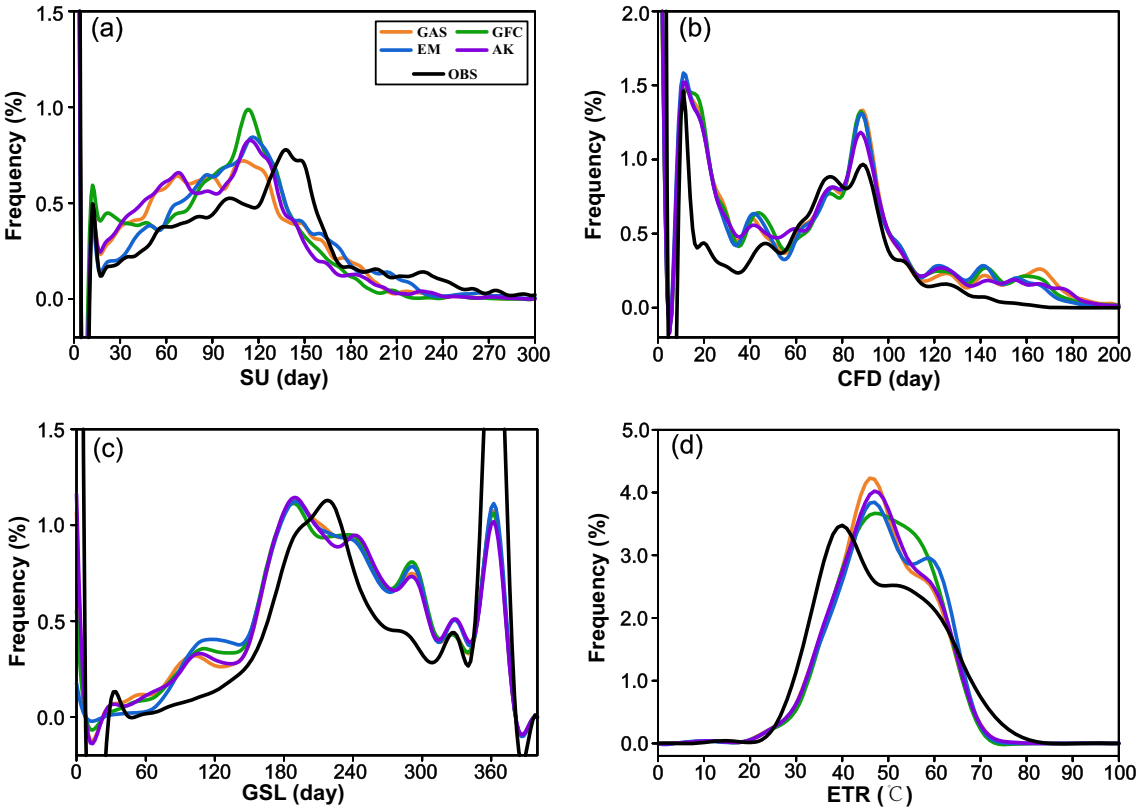

Fig. 15 Probability distribution functions for **a** SU, **b** CFD, **c** GSL, and **d** ETR. Equal bin size of 1.0 day is used in SU, CFD, and ETR analyses and 2.0 °C for GSL

firstly evaluated against the surface observation to examine their ability to simulate the regional precipitation climatology. Result shows that four CPSs can reproduce the spatial distribution of precipitation climatology. Analyzing the spatial variance of seasonal precipitation, the result shows that the precipitation distribution is better reproduced over the sub-regions in northern part of China. Among four CPSs, EM performs better in spring, summer, and autumn, and AK shows superiority in generating the precipitation distribution in winter. The ratios of convective to total precipitation by different CPSs are calculated, and GAS and GFC present much lower percentages of convective precipitation when AK produces the largest ratio. In simulating the PDFs of daily precipitation, all the CPSs perform well in the sub-regions of northeast and northwest China, but discrepancy among the four experiments and observation is evident over other sub-regions.

The simulated seasonal surface air temperatures by four CPSs are in good agreement with the observation but with the cold biases up to 8 °C. In the different sub-regions, in all CPS runs, the spatial distributions of seasonal temperature are reasonably reproduced. However, the convection-induced sub-grid circulation can affect the regional heating budget and lead to relatively large bias in summer temperature simulation over southeast and south China where the regional convective activities are strong. For PDFs of temperature, the bell-shaped or double peak patterns are well captured by all the CPSs. The shift towards the lower end of the temperature spectrum is in consensus with the cold bias in simulated temperature climatology.

In addition to regional climatology, the effect of CPSs on climatic extremes, which are represented by extreme temperature and precipitation indices, is analyzed as well. Results show that four CPSs can reasonably reproduce the overall patterns of extreme precipitation indices, but they display underestimation for CDD and overestimation for the three extreme precipitation indices. By comparing the simulated and observed trends of extreme precipitation indices, it can be concluded that CPSs can reasonably simulate the wetting tendency over Yangtze River and northwest China and the drying tendency over northeast and north China. The overall shapes of PDFs of extreme precipitation indices are correctly produced, but underestimation for dry events and overestimation for extreme precipitation events are evident in all CPS experiments. Comparably, AK scheme produces less error for probabilities of R10 and R95, and GAS exhibits a closer match to the observation in simulating probability distribution for Rx5.

Both simulated and observed spatial distributions of extreme temperature indices are in accordance with those of

annual mean temperature, and extreme warm events are correctly reproduced over the southeast China. In surface observation, the significant positive trends in the SU and GSL are detected, which are reasonably reproduced in CPS runs. AK scheme gives relatively better performance in portraying the trends of both CFD and ETR. The cumulus schemes have little impact on the spectrum distributions of extreme temperature indices, but the appearance of extreme warm events is underestimated.

In summary, our study emphasizes the influence of CPSs on both the temporal and spatial characters of regional climate. As the simulation focuses on China, whose climate is affected by (1) monsoon variabilities on different time scales and (2) strong topographical forcing. The paper analyzes the reactions of both summer and winter monsoon with the CPSs. Our study finds out that the summer monsoon system tends to have more complicated interactions with CPSs, which leads to large inter-CPS differences in summer precipitation simulation. In addition, by categorizing the simulation domain into eight sub-regions, we can study the CPSs' capabilities to simulate regional climate over regions with different land-surface characters and topography. The analysis shows that, over sub-regions with complex topography and inhomogeneous land-surface, such as southeast and southwest China, the option of CPS has great impact on model's accurate simulation of surface climate. The region has been experiencing surface warming during the past a few decades, which is clearly shown in both observation and simulation. Our simulation shows that all CPSs can more or less describe the effects of surface warming on sub-regional climatic extreme, the spatial variability, and trends of extreme indices, such as SU, R10, and R95, are sensitive to CPS.

Acknowledgments This work is part of the project National Basic Research and Development (973) Program of China (2010CB428500 and 2011CB952000) and supported by the National Natural Science Foundation of China (41375075 and 91425304). The authors also acknowledge with thanks the International Center for Theoretical Physics (ICTP) in Trieste Italy for providing the RegCM3 model. Observational data were provided by the China Meteorological Administration (CMA).

References

Alexander LV et al (2006) Global observed changes in daily climate extremes of temperature and precipitation. J Geophys Res Atmos 111:D05109. doi:10.1029/2005jd006290

Alexander LV, Pandora H, Dean C, Blair T, Amanda L, Neville N (2007) Trends in Australia's climate means and extremes: a global context. Aust Meteorol Mag 56:1–18

Anthes RA (1977) A cumulus parameterization scheme utilizing a one-dimensional cloud model. Mon Weather Rev 105:270–286

Bonnardot V, Cautenet S (2009) Mesoscale atmospheric modeling using a high horizontal grid resolution over a complex coastal terrain and a wine region of South Africa. J Appl Meteorol Climatol 48:330–348. doi:10.1175/2008jamc1710.1

Choi G et al (2009) Changes in means and extreme events of temperature and precipitation in the Asia-Pacific Network region, 1955–2007. Int J Climatol 29:1906–1925. doi:10.1002/joc.1979

Davis N, Bowden J, Semazzi F, Xie L, Önol B (2009) Customization of RegCM3 regional climate model for Eastern Africa and a tropical Indian Ocean domain. J Clim 22:3595–3616. doi:10.1175/2009jcli2388.1

Dickson R, Henderson-Sellees A, Kennedy P (1993) Biosphere–Atmosphere Transfer Scheme (BATS) version 1e as coupled to the NCAR community climate model. NCAR Tech. Note National Center for Atmospheric Research, Boulder

Dimri AP, Yasunari T, Wiltshire A, Kumar P, Mathison C, Ridley J, Jacob D (2013) Application of regional climate models to the Indian winter monsoon over the western Himalayas. Sci Total Environ 468:S36–S47. doi:10.1016/j.scitotenv.2013.01.040

Dong Q, Chen X, Chen T (2011) Characteristics and changes of extreme precipitation in the Yellow-Huaihe and Yangtze-Huaihe rivers basins, China. J Clim 24:3781–3795. doi:10.1175/2010jcli3653.1

Du H, Wu Z, Li M, Jin Y, Zong S, Meng X (2013) Characteristics of extreme daily minimum and maximum temperature over Northeast China, 1961–2009. Theor Appl Climatol 111:161–171. doi:10.1007/s00704-012-0649-3

Emanuel KA (1991) A scheme for representing cumulus convection in large-scale models. J Atmos Sci 48:2313–2335

Emanuel KA, Zivkovic-Rothman M (1999) Development and evaluation of a convection scheme for use in climate models. J Atmos Sci 56:1766–1782

Fan X, Wang Q, Wang M (2012) Changes in temperature and precipitation extremes during 1959–2008 in Shanxi, China. Theor Appl Climatol 109:283–303. doi:10.1007/s00704-011-0577-7

Fritsch JM, Chappell CF (1980) Numerical prediction of convectively driven mesoscale pressure systems. Part I: convective parameterization. J Atmos Sci 37:1722–1733

Fu C, Wei H, Chen M (1998) Simulation of the evolution of summer monsoon rainbelts over eastern China from regional climate model. Sci Atmos Sin 22:522–534

Fu C et al (2005) Regional climate model intercomparison project for Asia. Bull Am Meteorol Soc 86:257–266. doi:10.1175/bams-86-2-257

Gao X, Zhao Z, Giorgi F (2002) Changes of extreme events in regional climate simulations over East Asia. Adv Atmos Sci 19:927–942

Gianotti RL, Zhang D, Eltahir EAB (2011) Assessment of the regional climate model version 3 over the Maritime Continent using different cumulus parameterization and land surface schemes. J Clim 25:638–656. doi:10.1175/jcli-d-11-00025.1

Giorgi F, Marinucci MR, Bates GT (1993a) Development of a second-generation regional climate model (RegCM2). Mon Weather Rev 121:2794–2813

Giorgi F, Marinucci MR, Bates GT (1993b) Development of a second-generation regional climate model (RegCM2) part II convective processes and assimilation of lateral boundary conditions. Mon Weather Rev 121:2814–2832

Gong DY, Pan YZ, Wang JA (2004) Changes in extreme daily mean temperatures in summer in Eastern China during 1955–2000. Theor Appl Climatol 77:25–37. doi:10.1007/s00704-003-0019-2

Goswami BB, Mukhopadhyay P, Mahanta R, Goswami BN (2010) Multiscale interaction with topography and extreme rainfall events in the northeast Indian region. J Geophys Res Atmos 115. doi: 10.1029/2009jd012275

Grell GA (1993) Prognostic evaluation of assumptions used by cumulus parameterizations. Mon Weather Rev 121:764–787

Grell, Dudhia J, Stauffer D (1994) A description of the fifth-generation Penn State/NCAR Mesoscale Model (MM5) vol NCAR/TN-398+STR. NCAR Tech. Note

Gu H, Wang G, Yu Z, Mei R (2012) Assessing future climate changes and extreme indicators in east and South Asia using the RegCM4

regional climate model. Clim Chang 114:301–317. doi:10.1007/s10584-012-0411-y
Haylock M, Nicholls N (2000) Trends in extreme rainfall indices for an updated high quality data set for Australia, 1910–1998. Int J Climatol 20:1533–1541. doi:10.1002/1097-0088(20001115)20:13<1533::aid-joc586>3.0.co;2-j
Hegerl GC, Zwiers FW, Stott PA, Kharin VV (2004) Detectability of anthropogenic changes in annual temperature and precipitation extremes. J Clim 17:3683–3700. doi:10.1175/1520-0442(2004)017<3683:doacia>2.0.co;2
Heikkila U, Sandvik A, Sorteberg A (2011) Dynamical downscaling of ERA-40 in complex terrain using the WRF regional climate model. Clim Dyn 37:1551–1564. doi:10.1007/s00382-010-0928-6
Ho C-H et al (2011) A projection of extreme climate events in the 21(st) century over East Asia using the community climate system model 3. Asia-Pac J Atmos Sci 47:329–344. doi:10.1007/s13143-011-0020-0
Holtslag A, De Bruijin E, Pan H (1990) A high resolution air mass transformation model for short-range weather forecasting. Mon Weather Rev 118:1561–1575
Hu Y, Maskey S, Uhlenbrook S (2012) Trends in temperature and rainfall extremes in the Yellow River source region, China. Clim Chang 110:403–429. doi:10.1007/s10584-011-0056-2
Im E-S, Ahn J-B, Remedio AR, Kwon W-T (2008) Sensitivity of the regional climate of East/Southeast Asia to convective parameterizations in the RegCM3 modelling system. Part 1: focus on the Korean peninsula. Int J Climatol 28:1861–1877. doi:10.1002/joc.1664
Kang H-S, Hong S-Y (2008) Sensitivity of the simulated East Asian summer monsoon climatology to four convective parameterization schemes. J Geophys Res 113:D15119. doi:10.1029/2007jd009692
Kiehl JT, Hack JJ, Bonan G, Boville B, Briegleb B, Willamson D, Rasch P (1996) Description of the NCAR community climate model (CCM3) vol NCAR/TN-420+STR. NCAR Tech. Rep., National Center for Atmospheric Research, Boulder
Kuo YH, Reed RJ, Liu YB (1996) The ERICA IOP 5 storm.3. Mesoscale cyclogenesis and precipitation parameterization. Mon Weather Rev 124:1409–1434. doi:10.1175/1520-0493(1996)124<1409:teispi>2.0.co;2
Lee D-K, Suh M-S (2000) Ten-year East Asian summer monsoon simulation using a regional climate model (RegCM2). J Geophys Res 105:29565–29577
Lee DK, Cha DH, Choi SJ (2005) A sensitivity study of regional climate simulation to convective parameterization schemes for 1998 East Asian summer monsoon. Terr Atmos Ocean Sci 16:989–1015
Lee D-K, Cha D-H, Jin C-S, Choi S-J (2013) A regional climate change simulation over East Asia. Asia-Pac J Atmos Sci 49:655–664. doi:10.1007/s13143-013-0058-2
Lee J-W, Hong S-Y, Chang E-C, Suh M-S, Kang H-S (2014) Assessment of future climate change over East Asia due to the RCP scenarios downscaled by GRIMs-RMP. Clim Dyn 42:733–747. doi:10.1007/s00382-013-1841-6
Li Q, Wang Y (2012) Changes in the observed trends in extreme temperatures over China around 1990. J Clim 25:5208–5222. doi:10.1175/jcli-d-11-00437.1
Liu H, Wang B (2011) Sensitivity of regional climate simulations of the summer 1998 extreme rainfall to convective parameterization schemes. Meteorog Atmos Phys 114:1–15. doi:10.1007/s00703-011-0143-y
Liu Y, Giorgi F, Washington WM (1994) Simulation of summer monsoon climate over East Asia with an NCAR regional climate model. Mon Weather Rev 122:2331–2348
Liu Y, Avissar R, Giorgi F (1996) Simulation with the regional climate model RegCM2 of extremely anomalous precipitation during the 1991 East Asian flood. An evaluation study. J Geophys Res 101:26199–26215
Manton MJ et al (2001) Trends in extreme daily rainfall and temperature in Southeast Asia and the South Pacific: 1961–1998. Int J Climatol 21:269–284. doi:10.1002/joc.610
Moberg A, Jones PD (2005) Trends in indices for extremes in daily temperature and precipitation in central and Western Europe, 1901–99. Int J Climatol 25:1149–1171. doi:10.1002/joc.1163
Moberg A et al (2006) Indices for daily temperature and precipitation extremes in Europe analyzed for the period 1901–2000. J Geophys Res-Atmos 111:D05109. doi:10.1029/2006dj007103
Mukhopadhyay P, Taraphdar S, Goswami BN, Krishnakumar K (2010) Indian summer monsoon precipitation climatology in a high-resolution regional climate model: impacts of convective parameterization on systematic biases. Weather Forecast 25:369–387. doi:10.1175/2009waf2222320.1
Pal JS, Small EE, Eltahir EAB (2000) Simulation of regional-scale water and energy budgets: representation of subgrid cloud and precipitation processes within RegCM. J Geophys Res-Atmos 105:29579–29594. doi:10.1029/2000jd900415
Pal JS et al (2007) Regional climate modeling for the developing world—the ICTP RegCM3 and RegCNET. Bull Am Meteorol Soc 88:1395–1409. doi:10.1175/bams-88-9-1395
Qian W, Fu J, Zhang W, Lin X (2007) Changes in mean climate and extreme climate in China during the last 40 years. Adv Earth Sci 22:673–684
Qian Z, Hu J, Feng G, Cao Y (2012) Characteristics of the spatiotemporal distribution of daily extreme temperature events in China: minimum temperature records in different climate states against the background of the most probable temperature. Chin Phys B 21:109203-109201-109203-109208
Ratna SB, Ratnam JV, Behera SK, Rautenbach CJD, Ndarana T, Takahashi K, Yamagata T (2014) Performance assessment of three convective parameterization schemes in WRF for downscaling summer rainfall over South Africa. Clim Dyn 42:2931–2953. doi:10.1007/s00382-013-1918-2
Sato T, Xue Y (2013) Validating a regional climate model's downscaling ability for East Asian summer monsoonal interannual variability. Clim Dyn 41:2411–2426. doi:10.1007/s00382-012-1616-5
Singh GP, Oh J-H, Kim J-Y, Kim O-Y (2006) Sensitivity of summer monsoon precipitation over East Asia to convective parameterization schemes in RegCM3. SOLA 2:29–32. doi:10.2151/sola.2006-008
Sinha P, Mohanty UC, Kar SC, Dash SK, Kumari S (2012) Sensitivity of the GCM driven summer monsoon simulations to cumulus parameterization schemes in nested RegCM3. Theor Appl Climatol. doi:10.1007/s00704-012-0728-5
Su BD, Jiang T, Jin WB (2006) Recent trends in observed temperature and precipitation extremes in the Yangtze River basin, China. Theor Appl Climatol 83:139–151. doi:10.1007/s00704-005-0139-y
Tank A, Konnen GP (2003) Trends in indices of daily temperature and precipitation extremes in Europe, 1946–99. J Clim 16:3665–3680
Tank AMGK, et al (2006) Changes in daily temperature and precipitation extremes in central and south Asia. J Geophys Res Atmos 111. doi:10.1029/2005jd006316
Tchotchou LAD, Kamga FM (2009) Sensitivity of the simulated African monsoon of summers 1993 and 1999 to convective parameterization schemes in RegCM3. Theor Appl Climatol 100:207–220. doi:10.1007/s00704-009-0181-2
Tian Y, Xu Y-P, Booij MJ, Lin S, Zhang Q, Lou Z (2012) Detection of trends in precipitation extremes in Zhejiang, east China. Theor Appl Climatol 107:201–210. doi:10.1007/s00704-011-0472-2
Wang W, Seaman NL (1997) A comparison study of convective parameterization schemes in a mesoscale model. Mon Weather Rev 125:252–278. doi:10.1175/1520-0493(1997)125<0252:acsocp>2.0.co;2
Wang Z, Ding Y, Zhang Q, Song Y (2012) Changing trends of daily temperature extremes with different intensities in China. Acta Meteorol Sin 26:399–409. doi:10.1007/s13351-012-0401-z

Wang H, Chen Y, Xun S, Lai D, Fan Y, Li Z (2013) Changes in daily climate extremes in the arid area of Northwestern China. Theor Appl Climatol 112:15–28. doi:10.1007/s00704-012-0698-7

Williams CJR, Kniveton DR, Layberry R (2010) Assessment of a climate model to reproduce rainfall variability and extremes over Southern Africa. Theor Appl Climatol 99:9–27. doi:10.1007/s00704-009-0124-y

Xu X, Du Y, Tang J, Wang Y (2011) Variations of temperature and precipitation extremes in recent two decades over China. Atmos Res 101:143–154. doi:10.1016/j.atmosres.2011.02.003

Yan Z et al (2002) Trends of extreme temperatures in Europe and China based on daily observations. Clim Chang 53:355–392. doi:10.1023/a:1014939413284

Yang MJ, Chien FC, Cheng MD (2000) Precipitation parameterization in a simulated Mei-Yu front. Terr Atmos Ocean Sci 11: 393–422

Zanis P, Douvis C, Kapsomenakis I, Kioutsioukis I, Melas D, Pal JS (2009) A sensitivity study of the Regional Climate Model (RegCM3) to the convective scheme with emphasis in central eastern and southeastern Europe. Theor Appl Climatol 97:327–337. doi:10.1007/s00704-008-0075-8

Zhai PM, Zhang XB, Wan H, Pan XH (2005) Trends in total precipitation and frequency of daily precipitation extremes over China. J Clim 18: 1096–1108. doi:10.1175/jcli-3318.1

Zhang D-F, Ouyang L-C, Gao X-J, Zhao Z-C, Pal JS, Filippo G (2007) Simulation of the atmospheric circulation over east Asia and climate in China by RegCM3. J Trop Meteorol 23: 444–452

Zhang Y, Dulière V, Mote PW, Salathé EP (2009) Evaluation of WRF and HadRM mesoscale climate simulations over the U.S. Pacific Northwest*. J Clim 22:5511–5526. doi:10.1175/2009jcli2875.1

Zhang Q, Li J, Chen YD, Chen X (2011) Observed changes of temperature extremes during 1960–2005 in China: natural or human-induced variations? Theor Appl Climatol 106:417–431. doi:10.1007/s00704-011-0447-3